JGR Atmospheres

RESEARCH ARTICLE
10.1029/2021JD036071

Accurate Retrieval of Asymmetry Parameter for Large and Complex Ice Crystals From In-Situ Polar Nephelometer Measurements

Guanglang Xu[1], **Martin Schnaiter**[1], **and Emma Järvinen**[1]

[1]Karlsruhe Institute of Technology, Karlsruhe, Germany

Key Points:

- A new algorithm is developed for retrieving the asymmetry parameter of large and complex ice crystals from polar nephelometer measurements
- Accuracy of retrieval could be better than 0.01, provided sufficient smoothness of the phase function
- A case study of Arctic cirrus measurement during the CIRRUS-HL campaign is reported

Correspondence to:

G. Xu and E. Järvinen,
guanglang.xu@kit.edu;
emma.jaervinen@kit.edu

Citation:

Xu, G., Schnaiter, M., & Järvinen, E. (2022). Accurate retrieval of asymmetry parameter for large and complex ice crystals from in-situ polar nephelometer measurements. *Journal of Geophysical Research: Atmospheres*, *127*, e2021JD036071. https://doi.org/10.1029/2021JD036071

Received 19 OCT 2021
Accepted 20 JAN 2022

Author Contributions:

Conceptualization: Guanglang Xu
Data curation: Guanglang Xu, Emma Järvinen
Formal analysis: Guanglang Xu
Funding acquisition: Martin Schnaiter, Emma Järvinen
Investigation: Guanglang Xu
Methodology: Guanglang Xu
Project Administration: Martin Schnaiter, Emma Järvinen
Resources: Guanglang Xu, Martin Schnaiter, Emma Järvinen
Software: Guanglang Xu, Emma Järvinen
Validation: Guanglang Xu
Visualization: Guanglang Xu, Emma Järvinen

Abstract The retrieval of the asymmetry parameter from nephelometer measurements can be challenging due to the inability to detect the whole angular range. Here, we present a new method for retrieving the asymmetry parameter of ice crystals with relatively large size parameters (>50) from polar nephelometer measurements. We propose to fit the angular scattering measurement with a series of Legendre polynomials and the best fitted coefficients give the asymmetry parameter. The accuracy of the retrieval is analyzed by accessing the smoothness of the phase function, which is closely linked to the complexity of ice particle. It is found that the uncertainty of retrieval could be smaller than 0.01, provided the measured intensity profile is smooth enough. As an application, we report an case study on Arctic cirrus, which shows a mean value for the asymmetry parameter of 0.72.

Plain Language Summary The asymmetry parameter of ice crystals is a parameter that can largely determine cirrus cloud's interaction with solar radiation energy, and therefore its magnitude is important for climate and weather prediction models. In-situ measurements using nephelometers is a direct way to measure partial angular scattering functions, and the accuracy of these measurements is of upmost importance.
In this paper, we report a novel method for retrieving the asymmetry parameter from polar nephelometer measurements. Depending on the smoothness of the measured angular scattering function, the accuracy of the retrieval could be very high. We report a case study over the Arctic region, showing a low asymmetry parameter around 0.72.

1. Introduction

When solar radiation reaches the Earth's atmosphere, it is likely that the radiation is interacting with cirrus clouds, as they are formed in high altitudes and have a large coverage. At any moment, the coverage of cirrus cloud reach to approximately 40%–60% of the Earth's surface (Mace et al., 2009; Matus & L'Ecuyer, 2017; Sassen et al., 2008). It is recognized that cirrus's interaction with solar and infrared radiation will play a significant role in the energy balance of the Earth-atmosphere system (Liou, 1986, 1992; Stephens et al., 1990). At visible wavelengths, the radiative properties of cirrus are mainly determined by the ice crystal light scattering properties. Particularly, these properties define which fraction of the incoming radiation is redirected back into space and is therefore lost for the energy budget of the Earth. Hence, the so-called asymmetry parameter, characterizing the relative difference of the forward and backward scattered energy, needs to be determined. Although it contains only partial information of the angular scattering function, the asymmetry parameter is a key input parameter for the two-stream approximation of radiative transfer models (Liou, 2002). Because climate models mostly apply two-stream or Eddington approximations to parameterize radiative transfer (Fouquart et al., 1991; Randles et al., 2013), the asymmetry parameter of cirrus clouds largely determines their radiative impact in climate models (Fu, 2007; Kristjánsson et al., 2000; Liou, 2002).

The significance of the asymmetry parameter for cirrus clouds is also manifested by its connection to remote sensing (Labonnote et al., 2000; Yang et al., 2018). This can be revealed by a simple approximation formula of the plane-albedo of thin clouds (Liou, 2002; Meador & Weaver, 1980), that is,

$$R = \frac{\omega_0}{2\mu_0}(1-g)\tau, \tag{1}$$

Writing – original draft: Guanglang Xu
Writing – review & editing: Guanglang Xu, Martin Schnaiter, Emma Järvinen

where τ is the optical thickness, ω_0 is the scattering albedo, μ_0 is the cosine of direction of the incident solar radiation, and g is the asymmetry parameter of clouds. Because the optical depth is retrieved by measuring the reflected radiance for passive remote sensing, the assigned value of g (model value) for clouds, if not accurate, could induce large biases to the retrieval of optical thickness.

The asymmetry parameter of spherical particles, like water droplets, can be computed analytically due to their simplicity of shape. In contrast, ice crystals often exhibit complex shapes with a high degree of non-sphericity. This morphological complexity poses a great challenge for quantitatively studying their optical properties. Over the last few decades, progress has been made toward the improvement of the modeling capability of light scattering by non-spherical particles. Various techniques including the geometric-optics ray tracing and numerically accurate methods, such as the Improved Geometric Optics Method (IGOM), Discrete Dipole Approximation (DDA), Finite-Difference Time-Domain method (FDTD), Invariant Imbedding T-matrix method (II-TM), have been developed for modeling the light scattering properties of ice crystals (Bi & Yang, 2014; Macke et al., 1996; Mishchenko et al., 1996; Taflove & Umashankar, 1990; Yang & Liou, 1996a; Yang & Liou, 1996b; Yurkin et al., 2007). The merits of these methods include that they are theoretically sound, highly accurate, and have the abilities to predict and interpret observational data, particularly polarization data. However, the limitation that one has to make specific assumptions on the particle morphology often results in the use of idealized and simplified shapes, which most likely do not fully represent the optical properties of real atmospheric crystals with a high degree of morphological complexity.

Another approach for estimating the asymmetry parameter of cirrus clouds is to analyze the upwelling flux or multi-directional polarization data by applying radiation transfer theory and optical scattering models, for example, Stephens et al. (1990); Diedenhoven et al. (2012, 2013). The advantage of such analyses comprises the capability of probing cloud top information, being most relevant to the reflectance of clouds. As an indirect estimation, however, important assumptions on the cloud geometry (i.e., plane–parallel structure) has to be made for such analysis to be valid.

The most direct way of deriving the asymmetry parameter for ice crystals is the in-situ measurement by a nephelometer. Several instruments have been developed to measure the angular light scattering of ice crystals in-situ, including the Polar Nephelometer, Gayet et al. (1998) (PN), the Cloud Integrating Nephelometer (CIN), Gerber et al. (2000), and the Particle Habit Imaging and Polar Scattering (PHIPS) probe, Abdelmonem et al. (2016); Schnaiter et al. (2018). A common limitation of these instruments is the incapability to measure the whole angular range, particularly in the near-forward and near-backward scattering directions. Notably, by directly applying the cosine-weighted integral definition, Gerber et al. (2000) use CIN measurements to estimate the asymmetry parameter of cloud elements. In their approach, a fraction of energy in the forward scattering direction must be assumed in accordance with light scattering (diffraction) simulations. Other methods involving angular scattering measurements often use the best-fitting approach, by comparison with specific light scattering models, to determine the asymmetry parameter of ice crystals.

Despite decades of research, the value of the asymmetry parameter for ice crystals has not been very well constrained. If one asks the question what is the value of the asymmetry parameter for cirrus clouds, experimentalists and modellers will probably give different answers. Table 1 shows some typical values of g obtained from measurements and modeling studies. In general, the radiometer-based studies from the early 90s give quite low values of g, the CIN measurements tend to give values around 0.74–0.75. A typical range of 0.76–0.78 is reported from PN measurements and the modeling studies normally predict the asymmetry parameter above 0.8. The discrepancies between model and observation still motivate extensive studies of cirrus cloud optical properties, Bacon and Swanson (2000); Gerber et al. (2000); Liou and Yang (2016).

To further improve the accuracy of in-situ measurements, in this work, we developed a new method for retrieving the asymmetry parameter of ice crystals from polar nephelometer measurements with the PHIPS probe. The range of applicable size parameters (ratio of the characteristic length to the wavelength) is where geometric-optics treatments are applicable (Yang et al., 2013). In contrast to previous methods, our method avoids specific assumptions for the undetectable angular range, which removes biases that stem from the use of specific optical particle models.

The structure of this paper is as follows, in Section 2, we revisit the basic principles of nephelometer measurement of asymmetry parameter. In Section 3, we introduce the methodology for measuring asymmetry parameter

Table 1
Values of Asymmetry Parameter (g) Estimated From Measurement and Modeling Studies

g from radiometer/polarimeter observations	Reference
0.7	Stephens et al. (1990)
0.7	Stackhouse and Stephens (1991)
0.7	Wielicki et al. (1990)
0.75	Shiobara and Asano (1994)
0.76–0.78 (Tropical Cirrus, Florida)	Diedenhoven et al. (2012, 2013)
g from the Cloud Integrating Nephelometer (635 nm)	Reference
0.74 ± 0.03 (Arctic ice clouds)	Gerber et al. (2000)
	Garrett et al. (2001)
0.75 ± 0.01 (Florida anvil)	Garrett et al. (2003)
g from Polar Nephelometer	Reference
0.78–0.79 (Midlatitude cirrus, 800 nm)	Jourdan et al. (2003)
0.76–0.77 (Northern Hemisphere cirrus, 804 nm)	Gayet et al. (2004)
0.76–0.77 (Southern Hemisphere, 800 nm)	Shcherbakov et al. (2005)
0.77–0.78 (Midlatitude cirrus, 804 nm)	Mioche et al. (2010)
0.75 (Several cloud types, 532 nm)	Järvinen et al. (2018)
g from numerical models	Reference
0.79–0.88 (bullet rosettes)	Iaquinta et al. (1995)
0.80–0.92 (plates)	Macke et al. (1998)
0.77–0.86 (columns)	Macke et al. (1998)
0.76–0.77 (two-habit model)	Liu et al. (2014)

for PHIPS. In Section 4, we analyze the errors associated with the method. Section 5 reports the results from a recent in-situ measurements in Arctic cirrus clouds. Section 6 concludes this study.

2. Nephelometer Measurements of the Asymmetry Parameter

The asymmetry parameter g is defined as the cosine-weighted integral of the scattering phase function $P(\theta)$:

$$g = \int_0^{\pi} P(\theta)\cos(\theta)\sin(\theta)d\theta, \tag{2}$$

where θ is the scattering angle. As $\cos(\theta)$ has a maximum value of 1 at $\theta = 0$ and a minimum value -1 at $\theta = \pi$, g measures the relative difference between the forward-scattered and backscattered energy. This integral definition motivated the development of the CIN instrument Gerber et al. (2000), measuring the accumulated scattered energy by an ensemble of particles over a limited angular range (10–175°) with and without a "cosine mask". Specifically, the asymmetry parameter can be deduced from CIN measurements by the following expression:

$$g = f + \frac{cF - cB}{F + B}(1 - f), \tag{3}$$

where f is a constant number accounting for the energy within the forward-scattering range $\theta <= 10°$, cF and cB are the integrals of the "cosine-weighted" forward-scattering and backscattered energy respectively, while F and B denote the integration of forward-scattering and backscattered energy respectively without the "cosine mask." The advantage of the method is that the integration of the side-scattering energy could be accurate regardless of the smoothness of phase function. Nonetheless, this simple design also comes with some drawbacks. First, the error induced by the factor f is hard to quantify, because some light scattering models may not be sufficiently accurate to reproduce the scattering phase function of real ice crystals due to morphological complexities across different scales. Second, for each cloud type, one has to assume a different value of f, which increase the complexity

of the retrieval algorithm. Generally, depending on the cloud microphysical properties, the absolute error could be around 0.04 for CIN. It should be noted that Equation 3 can also be applied to retrieve asymmetry parameter from polar nephelometer measurements Auriol et al. (2001).

Another approach for estimating the asymmetry parameter is to use statistical inversion method, Jourdan et al. (2003). This method requires the building of a look-up table based on light scattering simulations, which is essentially a best-fitting approach. The merits of such approach include that it can generate multiple parameters simultaneously, such as extrapolated scattering phase function, extinction coefficient, asymmetry parameter and scattering albedo. Nevertheless, the retrieved parameters will be inevitably biased toward the pre-computed look-up table.

It can be seen that the existing algorithms for estimating the asymmetry parameter of ice crystals rely on simulated optical properties of specific hexagonal models. The limitation of such approach is obvious, that is, as the level of complexity of real ice crystal increases, the model may not be representative anymore. This will inevitably introduces biases for the retrieval of asymmetry parameter, making the accuracy assessment intractable. This limitation is unlikely to be resolved by simply improving the accuracy of measurement. Instead, an algorithm that minimizes the dependence on light scattering simulations needs to be designed, which is the main objective of this study.

3. Methodology

We start by expanding arbitrary phase function $P(\theta)$ in terms of series of Legendre polynomials $P_l(\cos(\theta))$ Wiscombe (1977),

$$P(\theta) = \sum_{l=0}^{\infty} (2l+1)\hat{c}_l P_l(\cos(\theta)), \tag{4}$$

where $\hat{c}_l$ denotes the expansion coefficient of degree l. Due to the orthogonal property of Legendre polynomials, the expansion coefficient $\hat{c}_l$ can be evaluated by the following integral,

$$\hat{c}_l = \frac{1}{2}\int_{-1}^{1} P(\theta)P_l(\cos(\theta))d(\cos(\theta)) \tag{5}$$

Let the phase function be normalized to 4π, that is,

$$\int_0^{2\pi}\int_0^{\pi} P(\theta)\sin(\theta)d\theta d\phi = 4\pi, \tag{6}$$

it follows that

$$\hat{c}_0 = 1, \tag{7}$$

and $\hat{c}_1$ equals to the asymmetry parameter,

$$\hat{c}_1 = g, \tag{8}$$

meaning that asymmetry parameter is the first moment of scattering phase function with respect to Legendre polynomial.

For ice crystals whose size is large compared to incident wavelength, geometric optics ray-tracing approximation can be applied to calculate the optical scattering properties (Macke et al., 1996; Yang & Liou, 1996b). The scattering phase function is contributed by two separate parts, the external diffraction and ray-tracing part. The ray-tracing part of scattering phase function, accounting for reflection and refraction of light rays, is what a polar nephelometer can measure practically. According to the principle of light scattering in geometric-optics regime, the diffraction and ray-tracing contribution will be asymptotically equal when particle size parameter becomes large Yang et al. (2013). In this study, we set this lower limit of size parameter to be 50. For PHIPS probe, with a laser beam of wavelength 532 nm, this lower limit of particle size is round 26 μm. In this range, the scattering phase function can be approximately written as Macke et al. (1996):

$$P(\theta) = \frac{1}{2\omega_0}\left[(2\omega_0 - 1)\, P_{GO}(\theta) + P_D(\theta)\right], \tag{9}$$

where $P_{GO}(\theta)$ denotes the geometric-optics ray-tracing contribution and $P_D(\theta)$ is the external diffraction contribution, and ω_0 is the single scattering albedo. The well-known 22-degree and 46-degree halo produced by pristine hexagonal cylinders are due to the contribution of $P_{GO}(\theta)$. More specifically, it can be explained by the light rays refracted through prism angles of 60° and 90°, respectively. For complex real ice crystals, the phase function P_{GO} is generally featureless. $P_D(\theta)$ can be calculated by an integral involving the geometric projection of the particle along the incident direction, resulting a highly forward-peaked phase function. Previously, to estimate the value of g, a fraction of energy has to be assumed constant (~0.56) to account for the undetectable angular range of $\theta < 10°$, which is dominated by diffraction contribution $P_D(\theta)$ Gerber et al. (2000).

Applying the Legendre expansion to Equation 9, one can obtain the following relation for the corresponding expansion coefficients,

$$\hat{c}_l = \frac{1}{2\omega_0}\left[(2\omega_0 - 1)\, \hat{c}_{GO,l} + \hat{c}_{D,l}\right], l = 0, 1, 2, \ldots \tag{10}$$

where $\hat{c}_{GO,l}$ and $\hat{c}_{D,l}$ are the expansion coefficients for geometric-optics and diffraction phase function respectively. Take $l = 1$, we have the relation for asymmetry parameter,

$$g = \frac{1}{2\omega_0}\left[(2\omega_0 - 1)\, g_{GO} + g_D\right], \tag{11}$$

where $g_{GO} = \hat{c}_{GO,1}$ and $g_D = \hat{c}_{D,1}$ are the asymmetry parameter contributed by geometric-optics and diffraction respectively. As the diffraction phase function is highly peaked, g_D is very close to unity. According to the analysis of scalar diffraction (SD) theory (Bohren & Huffman, 2008), the diffraction pattern for a spherical aperture shall have the following form:

$$P_{\mathrm{SD}}(\theta) \propto (1 + \cos(\theta))^2 \left(\frac{J_1(x\sin(\theta))}{x\sin(\theta)}\right)^2, \tag{12}$$

where x is particle size parameter, and J_1 is the first order Bessel function. According to the analysis in Mishchenko et al. (2002), most of the diffracted energy will be confined into the angular range of $\theta < 7/x$ (in radian), which is a small angular range for ice crystals that are large enough. Despite that the above analysis is valid for spherical particle, the error caused by non-spherical ice crystal should be small as well since the asymmetry parameter due to large particle diffraction is very close to unity. We therefore make the following assumption,

$$P_D(\theta) = P_{\mathrm{SD}}(\theta). \tag{13}$$

To facilitate the retrieval, we computed the value of g_D as a function of particle size d in μm using Equation 12, where d is defined as,

$$d = \frac{x\lambda}{\pi}, \tag{14}$$

where $\lambda = 0.532$ μm is the wavelength used for measurement. The results are displayed in Figure 1. On logarithmic scale, $g_D(d)$ can be approximated by a polynomial of degree 4, that is.,

$$\begin{aligned} g_D(d) = &-5.9270 \times 10^{-5} - 0.00130 \times \ln(d) - 0.01087 \times (\ln(d))^2 \\ &+0.04093 \times (\ln(d))^3 + 0.94029 \times (\ln(d))^4. \end{aligned} \tag{15}$$

The above fitting uses particle size range from 3.3 to 846.7 μm, which covers most the size range in our measurement. For particle being larger than the upper limit, the value at 846.7 μm is used. In practice, the lower limit for Equation 12 to be valid is assumed to be 26 μm. It can be seen that g_D is a weakly varying function with respect to particle size, resulting a relatively small error of 0.005 for the estimation of asymmetry parameter. Exploiting this weakly varying feature of diffraction contribution is important, because we can mainly focus on analyzing the error due to the integration associated with the geometric-optics phase function $P_{GO}(\theta)$, which will be discussed

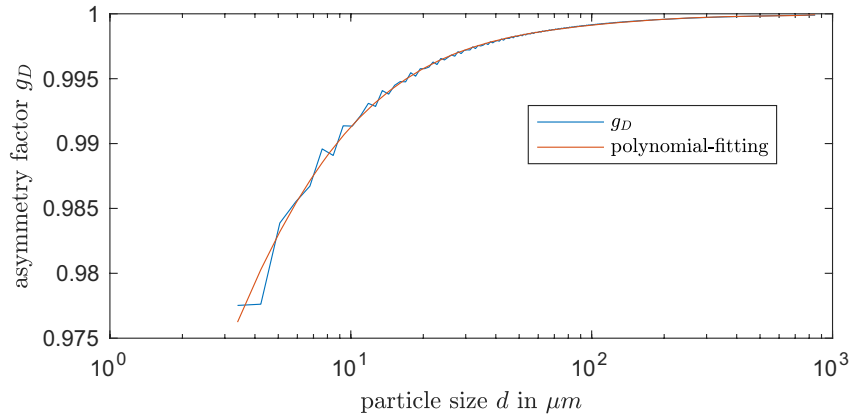

Figure 1. Asymmetry parameter g_D as a function of particle size d.

in the next section. We note that van Diedenhoven et al. (2014) also gives a empirical relation between the g_D and size parameter x based on diffraction computation of hexagonal ice crystal of specific aspect ratio.

In the following, we shall find a set of Legendre polynomial coefficients up to degree N_t, giving the best-fit to the measured angular intensities. By doing so, we automatically obtain the asymmetry parameter g_{GO}. Let a series of coefficients denoted by

$$\vec{c_{GO}} = \left(c_{GO,0}, c_{GO,1}, c_{GO,2}, \ldots, c_{GO,N_t}\right). \tag{16}$$

The problem can be cast as the following optimization problem:

$$\arg\min_{\vec{c_{GO}}} \sigma\left(\vec{c_{GO}}\right) := \sum_{n=1}^{N_m}\left(\sum_{l=0}^{N_t} c_{GO,l} P_l\left(\cos\left(\theta_n\right)\right) - I\left(\theta_n\right)\right)^2, \tag{17}$$

where $I(\theta_n)$ is the measured intensity from the polar nephelometer at scattering angle θ_n, and N_m is the total number of measurement directions. We then can obtain the normalized coefficients and the asymmetry parameter by the following formula:

$$\hat{c}_{GO,l} = \frac{c_{GO,l}}{c_{GO,0}}, l = 0, 1, \ldots, N_t. \tag{18}$$

The above optimization problem can be converted to a system of linear equations, and solved by using least-squared-fitting formula, see for example, Hu et al. (2000). Nevertheless, for arbitrary phase function to converge, N_t should be large enough. This could cause numerical instability, as large matrix inversion will be involved. To circumvent this difficulty, we first compute the intensity $I(\arccos(x_i))$ at Gauss–Legendre quadrature node x_i via interpolation and extrapolation of $I(\theta_n)$, and the coefficients of various degrees can be then computed precisely via Gauss–Legendre quadrature integration:

$$c_{GO,l} = \frac{1}{2}\sum_{j=1}^{N_t} I\left(\arccos\left(x_j\right)\right) P_l\left(x_j\right) w_j, \tag{19}$$

where w_j are the weights with respect to the quadrature.

As suggested by Equation 15, the asymmetry parameter, in other words, the first moment of diffraction phase function can be derived from particle size distribution (PSD). The PSD information is available from PHIPS probe since, besides recording single-particle angular scattering functions, stereo-microscopic images are also recorded. Now we can summarize our proposed method in the following flowchart (Figure 2):

Note that by finding the expansion coefficients, we not only retrieve asymmetry parameter, but also recover the phase function at arbitrary scattering angle. In the next section, we shall see that obtaining a set of best-fitting coefficients is crucial for analyzing the accuracy of retrieval.

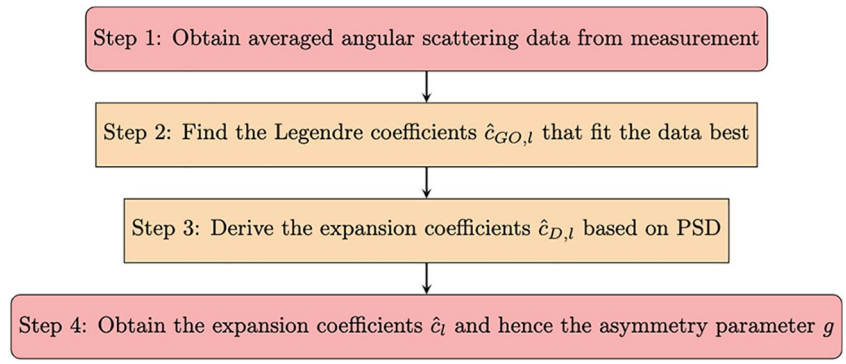

Figure 2. Method for retrieving asymmetry parameter from measurement.

The key ingredients of our method include two parts, one is the data fitting with Legendre polynomials, and second is the computation of diffraction expansion coefficients. Because the diffraction phase function is highly peaked, the expansion of such phase function requires many terms (could be larger than 6,000). To circumvent this difficulty, one can approximate the diffraction pattern by the Henyey–Greenstein (H–G) phase function van de Hulst (1980), as the HG function is completely determined by the asymmetry parameter. In such way, the phase function expansion can be written as:

$$\hat{c}_l = \frac{1}{2\omega_0}\left[(2\omega_0 - 1)\,\hat{c}_{GO,l} + g_D(x)^l\right], l = 0, 1, 2, \ldots, . \tag{20}$$

It is interesting to see that Equation 20 explicitly contains many parameters that are relevant to light scattering, the asymmetry parameter, scattering albedo ω_0, and size parameter x. Implicitly, $\hat{c}_{GO,l}$ are largely determined by the particle morphology. These coefficients are useful in radiative transfer computation, and now they can be derived from the polar nephelometer measurements.

4. Error Analysis

We shall now discuss the accuracy of the method. In practice, multiple error sources for the estimation of asymmetry parameter could exist, including factors that are associated with instruments, noise of measurements, shattering and so on. As we are mainly concerned with the problem of designing an algorithm, in this part, we will be focusing on the errors that are associated with the algorithm described in the last section.

4.1. Integration Error

The retrieval of asymmetry parameter from nephelometer is nothing but performing integration based on an incomplete angular-intensity profile. For polar nephelometer measurement, interpolation of the intensity is necessary. It is apparent that the accuracy of interpolating the intensities (i.e., $P_{GO}(\theta)$) will be largely determined by its characteristics, such as whether a peak or sharp-change of intensity appears at small scattering angle and the halos that appears in pristine hexagonal crystals. Despite that the measured phase function (e.g., 18°–170°) is very often featureless, it is uncertain how much error will be induced by applying Equation 19. A basic property of Gauss–Legendre quadrature is that the integration is exact provided that the integrand can be represented using polynomials of degree up to $N = 2n_t - 1$, where n_t is the number of quadrature weights or nodes used. If N is a relatively small number, the quadrature nodes could be well confined in the range of detection, resulting a highly accurate estimation of asymmetry parameter. In the following, we shall exploit this fact for the purpose of error estimation.

In accordance with Equations 19 and 18, taking $l = 1$, we have the following expression for g_{GO}:

$$g_{GO} = \frac{\sum_{j=1}^{n_t} I\left(\arccos\left(x_j\right)\right) x_j w_j}{\sum_{j=1}^{n_t} I\left(\arccos\left(x_j\right)\right) w_j}. \tag{21}$$

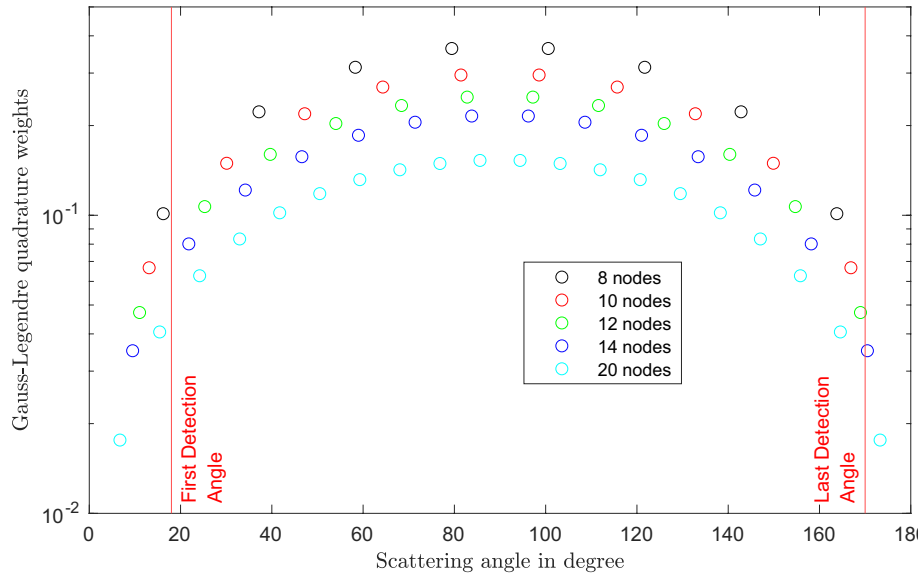

Figure 3. The angular detection range of PHIPS and the Gauss–Legendre quadrature weights when different number of nodes are used.

It can be seen that the value of g_{GO} will be exact as long as the intensity $I(\theta)$ can be represented using polynomials of degree up to $N = 2n_t - 2$, because we have a term $I(\arccos(x_j))x_j$ in the numerator. Accordingly,

$$I(\theta) = Const. \times \sum_{l=0}^{N}(2l+1)\hat{\alpha}_l P_l(\cos(\theta)), \tag{22}$$

where a *Constant* is assumed such that $\hat{\alpha}_0 = 1$. This constant is irrelevant for the analysis due to Equation 21. The accuracy of integration must be limited by the accuracy of approximating $I(\theta)$ using Equation 22. In general, we can use the following term associated with the last coefficient to access the accuracy of approximation,

$$\varepsilon = (2N+1)|\hat{\alpha}_N|. \tag{23}$$

Hence, given a small coefficient $|\hat{\alpha}_N|$, the error is proportional to $(2N+1)$.This suggests that the method will obtain its best accuracy only if the expansion coefficient decays fast enough to small magnitude. In other words, the decay rate of the expansion coefficient is a determining factor for the integration to be accurate. As we shall see in a moment, this feature has very close relation with the morphological complexity of ice crystals. Let us require that:

$$\varepsilon \leq 0.001, \tag{24}$$

which leads to

$$|\hat{\alpha}_N| \leq \frac{0.001}{2N+1}. \tag{25}$$

We note that the upper limit of N is crucial for accessing the accuracy for PHIPS. This is because the number of N directly determines the Gauss–Legendre nodes and weights to be used in the integration. Remember that a common limitation of current polar nephelometers is that they are not able to measure the whole angular range. For PHIPS, the detection range is from 18° to 170° with 20 detectors equally spaced. For the integration to be accurate, the corresponding Gauss–Legendre nodes shall be mostly within the range of detection. Figure 3 displays the Gauss–Legendre quadrature weights when different number of nodes are used. The two vertical lines indicate the detection range of PHIPS. It is not difficult to see that the best scheme for PHIPS is to be able to use no more than 8 nodes for integration, which lead to

$$N \leq 14. \tag{26}$$

And therefore,

$$|\hat{\alpha}_N| \leq 3.448 \times 10^{-6}. \tag{27}$$

In other words, for PHIPS, if the measured intensity profile can be approximated by Equation 22 with $N = 14$, to such an extent that its expansion coefficient $\hat{\alpha}_l$ decays to a magnitude of 3.448×10^{-6}, the error associated with the asymmetry parameter should be around the order of 0.001.

4.2. Connection With Particle Morphological Complexity

As suggested by the above analysis, the decay rate of the expansion coefficients is a determining factor for the accuracy of retrieval. A natural question is, how to measure the decay rate of the expansion coefficient?

The decay rate of the expansion coefficient actually links to the smoothness, or the simplicity, of phase function. It has been well recognized that the morphological complexity of ice crystals, such as surface roughness, air-bubble inclusion will "smooth" the scattering phase function compared to a pristine counterpart. In modeling studies, attempts have been made to characterize these complexities, such as the distortion parameters and surface roughness parameter applied in Macke and Yang's ray tracing codes (Macke et al., 1996; Yang et al., 2008). In addition, Gaussian random spheres can produce smooth phase functions (Muinonen et al., 1996). These metrics are largely equivalent in terms of the effects on phase function. Nevertheless, these complexity metrics are designed for light scattering simulation, not retrievable by a polar nephelometer. Hence the complexity metrics such as the distortion parameter are not applicable for accessing the accuracy of our algorithm.

It turns out that following parameter is useful to measure the decay rate of the expansion coefficient:

$$C_p = \left(\sum_{l=0}^{\infty} |\hat{c}_{GO,l}| \right)^{-1}. \tag{28}$$

In practice, C_p can only be estimated by a truncated series of Legendre polynomials. To our surprise, the value of C_p is closely related to the distortion parameter, δ, designed for ray-tracing computation. The upper panel of Figure 4 shows the scattering phase functions of a hexagonal columnar particle with different C_p values. Different C_p values are calculated by varying the distortion parameter in the ray-tracing code. As displayed in the figure, the halo produced by pristine hexagonal column corresponds to $C_p = 0.01$. As the value C_p increases, the halo disappears in the scattering phase function. The lower panel of Figure 4 displays the relation between the distortion parameter and C_p for various hexagonal columns and plates, where R denotes radius and L denotes the length in μm. It can be seen that relation is very close to a linear proportional relation, suggesting strong correlation between the two. Therefore, the value of C_p can also be used as an indicator of the degree of complexity of ice crystals. What being more useful in practice is that it is retrievable by a polar nephelometer.

In the following, we discuss some basic properties of C_p. For arbitrary normalized phase function, C_p satisfies the following relation:

$$0 \leq C_p \leq 1. \tag{29}$$

The values of 0 and 1 correspond to a Dirac delta function (i.e., no scattering) and isotropic scattering phase function respectively. This is due to the following relation:

$$2\delta(1 - \cos(\theta)) = \sum_{l=0}^{\infty} (2l + 1) P_l(\cos(\theta)), \tag{30}$$

meaning $\hat{c}_{GO,l} = 1$ for all l, which makes the value of C_p infinitely close to *zero*. On the other hand, for a constant phase function, we have:

$$\hat{c}_{GO,l} = \begin{cases} 1 & \text{if } l = 0, \\ 0 & \text{if } l > 0, \end{cases}$$

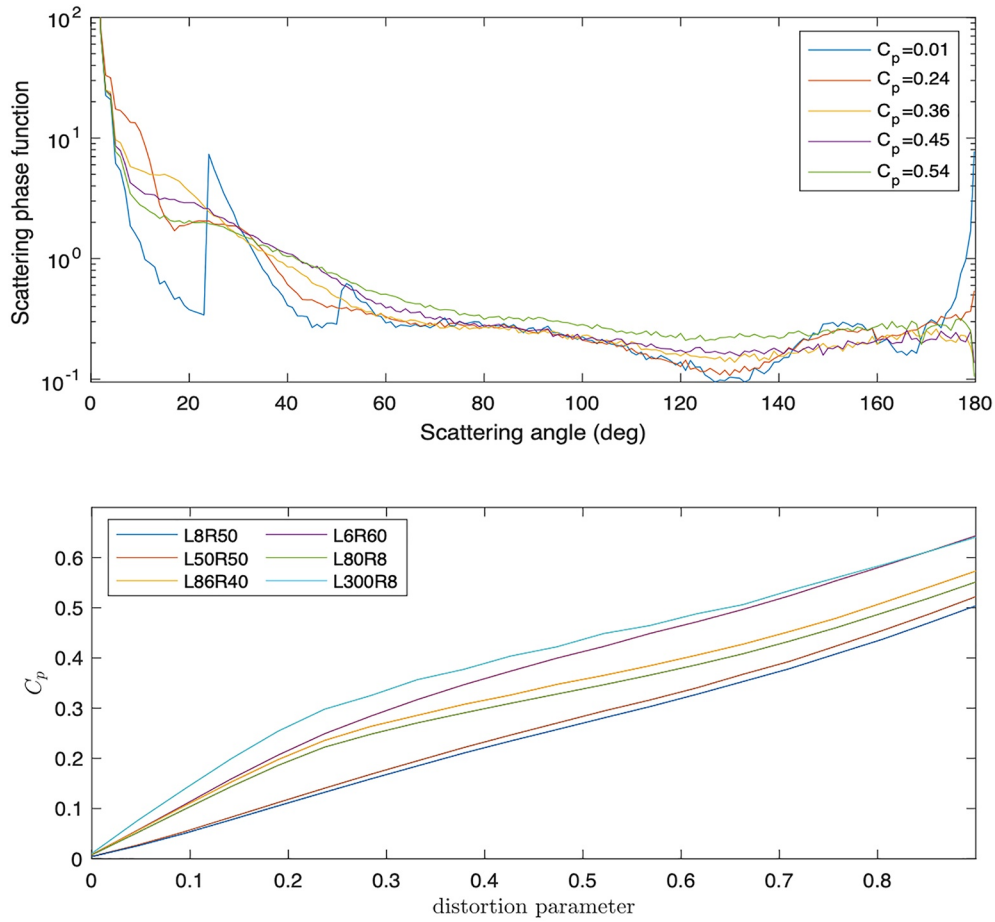

Figure 4. The correlation of C_p and distortion parameter applied in Macke's ray-tracing code.

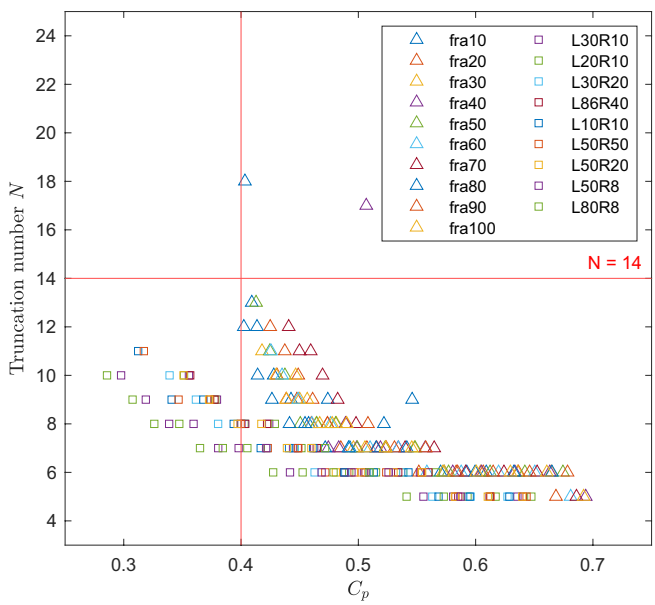

Figure 5. Number of truncation term N associated with truncation error $\varepsilon = 0.001$, as a function of C_p for different ice crystal scattering models.

which leads to $C_p = 1$. For the H-G phase function, we have

$$C_p = \left(\sum_{l=0}^{\infty} |g^l| \right)^{-1} = 1 - |g|. \tag{31}$$

Observe that for H–G phase function, the value of C_p is always inversely proportional to the asymmetry parameter with constant ratio of -1, while this is not true for the scattering of real ice crystals. As a matter of fact, based on simulations, the relation between C_p and asymmetry parameter g is complicated and closely related to the aspect ratio of the particle (see Figure 10). For aspect ratio close to unity, the asymmetry parameter, as the first moment of the phase function, decays rather slowly in the region of small C_p. We shall discuss this in more detailed in the next section.

The introduction of the auxiliary parameter C_p is an important component of our method, because it can be simultaneously estimated with asymmetry parameter and serves the purpose of accessing the accuracy. Figure 5 displays the number of truncation terms N associated with an error of 0.001 (Equation 26), as a function of C_p for different light scattering models. The legend of *fra*100, for example, denotes the model of a second generation random fractal shape with radius of 100 μm. There are two branches of points associated with two different models. The upper branch is associated with the *fractal* model (denoted by *triangle*), while the lower branch is associated with

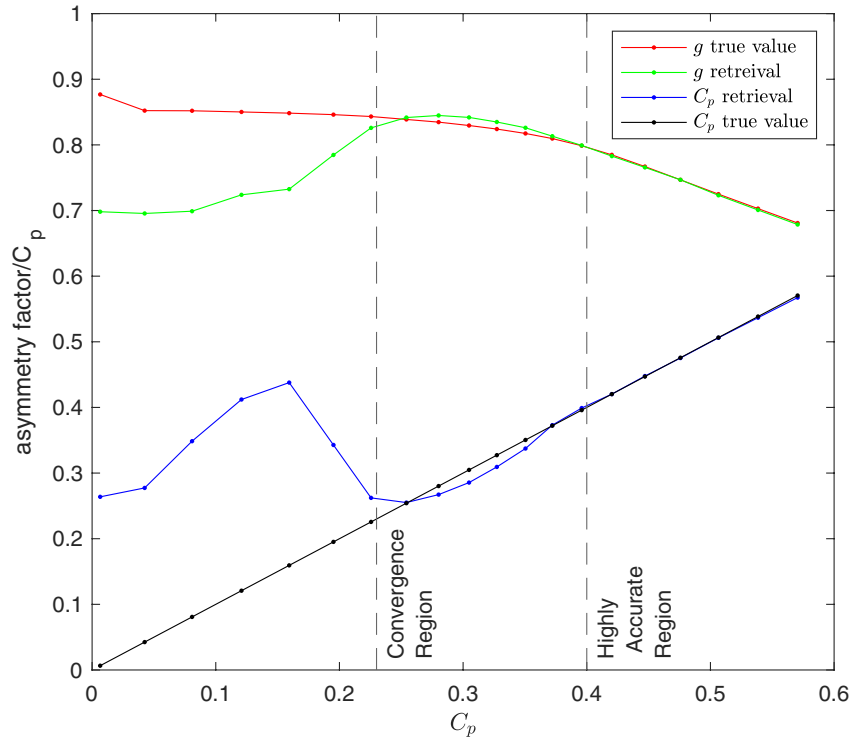

Figure 6. C_p and its corresponding asymmetry parameter for a mixture of different models and their retrieval results based on our method.

the *hexagonal* models (denoted by *square*). It can be seen that for most of the models, the number of truncation term N is smaller than 14 as $C_p > 0.4$. In other words, if C_p large than 0.4, the error of retrieval shall be at the order of 0.001.

Numerical experiment has been carried out to further verify this observation. For example, in Figure 6, the red and black curves show the true values of asymmetry parameter and C_p, respectively, while the green and blue curves are the corresponding retrieval values. We note that the true values are calculated based on the mixing of the six models used in Figure 4. It can be seen that when $C_p < 0.23$, large bias could be induced. This is because in this region, a large number of truncation term is needed to accurately represent the phase function. When $0.23 \leq C_p \leq 0.4$, the error of retrieval starts to converge. When $C_p > 0.4$, the retrieval becomes highly accurate, which is consistent with our analysis. Based on Figure 6, we can further observe that: (a) Both estimated value of asymmetry parameter and C_p will converge to its true value; (b) The asymmetry parameter is generally negatively correlated with C_p as C_p becomes large enough (e.g., $C_p > 0.4$), and this could be used as an additional constrain for our retrieval.

4.3. Other Error Sources

For geometric-optics treatment to be applicable, we have set a lower limit of particle size to be 26 μm, corresponding to a size parameter of 50 at wavelength 532 nm. The error associated with this limit can be estimated by Mishchenko et al. (2002):

$$O\left(x^{-3/2}\right) = O\left(50^{-3/2}\right) = 10^{-3}. \tag{32}$$

In practice, the particle size is generally larger than this limit.

For the Gauss–Legendre quadrature to be used for integration, the intensities at the corresponding nodes must be known. Nonetheless, for many of the polar nephelometer, including PHIPS, the detectors used for measuring the intensity are often placed equally spaced. This leads to a potential error caused by interpolation or extrapolation. Such an error is presumably small, provided that the phase function is smooth enough after averaging. To

avoid potential bias of interpolation/extrapolation, we use the average value obtained from multiple interpolation methods. Specifically,

$$I\left(arcos\left(x_i\right)\right) = \frac{1}{3}\left(I_{nearest} + I_{linear} + I_{cubic}\right), \tag{33}$$

where $I(arcos(x_i))$ is the intensity to be used for Gaussian quadrature, and $I_{nearest}$, I_{linear} and I_{cubic} are the interpolation intensities based on the *nearest* − *point*, *linear*, and *cubic* interpolation methods, respectively. Numerical experiments have been carried out to verify the accuracy of the scheme (as seen in Figure 6). It should be noted that as C_p becomes close to or larger than 0.4, the value of integration becomes rather invariant to the interpolation methods. In other words, different interpolation methods will give the same value. The extrapolation to small angles based on Equation 33 serve the purpose of estimating the value of C_p. It is worth noting that the interpolation error could be voided if the detector is placed according to the Gauss–Legendre nodes.

In addition, we note that to avoid contamination by diffraction, the first small detection angle θ_1 should satisfy

$$\theta_1 \geq \frac{7}{x}, \tag{34}$$

where x is the particle size parameter. Assuming a lower limit of $x = 50$, the optimal number of nodes to be used is $n_t = 16$ and $\theta_1 = 8.35°$.

Apart from the error associated with the algorithm, in practice, the errors caused by instrument design, sensors, noises, data processing, could potentially be important. A discussion of these issues is beyond the scope of this paper, more information can be seen in Baumgardner et al. (2017). To briefly summarize this section, we analyze the error of integration by introducing the C_p parameter, measuring the smoothness of the angular intensity profile. It is found that when $C_p > 0.4$, the accuracy could reach to about 10^{-3}. We also found a strong correlation between C_p and the distortion parameter defined in the ray-tracing model, which suggests that high morphological complexity gives high accuracy of retrieval.

5. A Case Study of an Arctic Cirrus

As an application of our method, we report the results from a case study of Arctic cirrus sampled on June 29, 2021 during the CIRRUS in High-Latitude (CIRRUS-HL) campaign when measurements flights were made in natural and aviation influenced cirrus using the DLR HALO aircraft equipped with a suite of in-situ and remote sensing instruments. The in-situ instrumentation included the PHIPS probe for characterization of the ice crystal angular light scattering properties. On the day of the case study, a warm front associated with southwesterly flow on the east coast of Greenland generated high level clouds north and northeast of Iceland. A thick Arctic cirrus cloud layer reaching from 8.8 to 11.3 km was observed and sampled in-situ on six different altitudes that were Langragrian to the airflow. Weather forecast prior to the sampling showed ascending air masses indicating a potential liquid origin for the cirrus ice crystals.

5.1. Time Series of Temperature and Ice Crystal Properties

Figure 7 shows a time series of the flight altitude and temperature (panel a), the ice crystal the area-equivalent diameter derived from the PHIPS stereo-microscopic images (panel b) and the corresponding values for C_p (panel b) and asymmetry parameter (panel d). Each data point in these panels represents an ensemble measurements of 20 consecutive single-particle events. It is assumed that there is no preferred particle orientation in these populations.

Largest ice crystal sizes were observed in the lowest sampling levels (between 8.8 and 9.5 km, −35°C and −39°C) where ice crystals with mean diameters up to 182 μm were observed. Stereo-microscopic images showed that the lowest sampling levels were dominated by compact and highly irregular crystals showing plate like growth with occasional bullet rosettes embedded. Panel I in Figure 8 shows example crystals from a period between 10:16:09 and 10:16:56 UTC that is highlighted with letter I in Figure 7. The ice crystal diameter, C_p value and g are highlighted with increased symbol size in the corresponding panels. During this period 53 stereo-images of

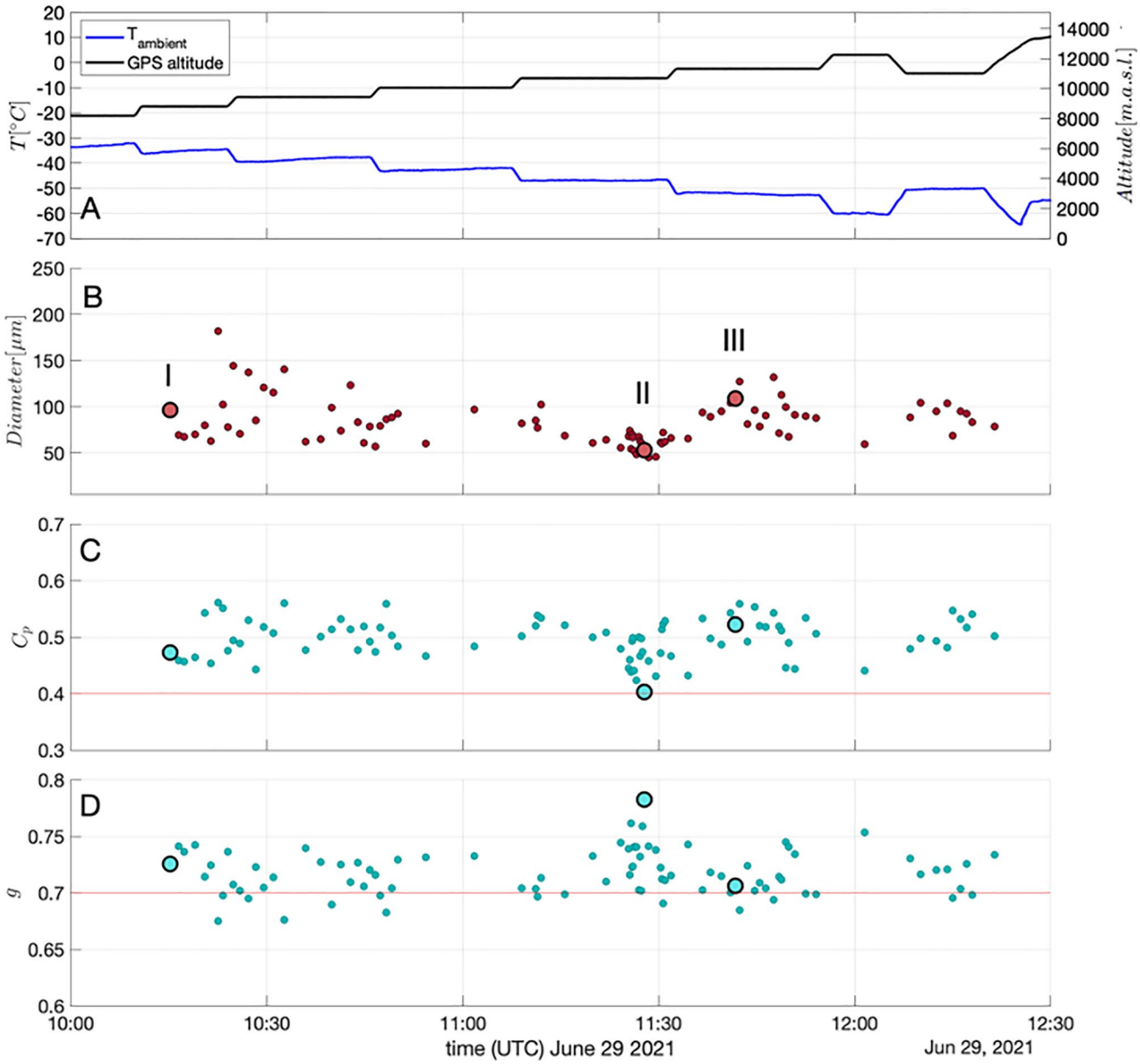

Figure 7. Application of the proposed method for retrieving the parameter C_p and asymmetry parameter g in CIRRUS-HL with PHIPS instrument, on June 29, 2021. The panel (a) shows the ambient temperature in degree Celsius together with the GPS altitude, the panel (b) the mean diameter of the crystal population, the panel (c) the complexity parameter C_p and the panel (d) the values for g for the same population.

ice crystals were acquired, from which 53% were manually classified as irregular crystals, 13% as side-planes, 26% showed indication of shattering and the rest (8%) were incompletely imaged and could not been classified.

After 1043 UTC mostly bullet rosettes and small compact crystals, that partly resembled sublimated bullet rosettes, were observed. The average diameter was predominantly below 100 μm. Panel II in Figure 8 shows example crystals from a period between 11:27:38 and 11:28:00 UTC, when compact and sometimes even quasi-spherical crystals were observed. This period included 27 stereo-microscopic images, from which 41% were manually classified as quasi-spherical crystals, 30% as bullet rosettes, 19% as irregular and the rest (10%) could not be classified. All of the observed bullet rosettes showed indications of sublimation and simultaneous RH measurements (not shown here) confirmed occasional periods of sub-saturated conditions that might have contributed to sublimation of these crystals.

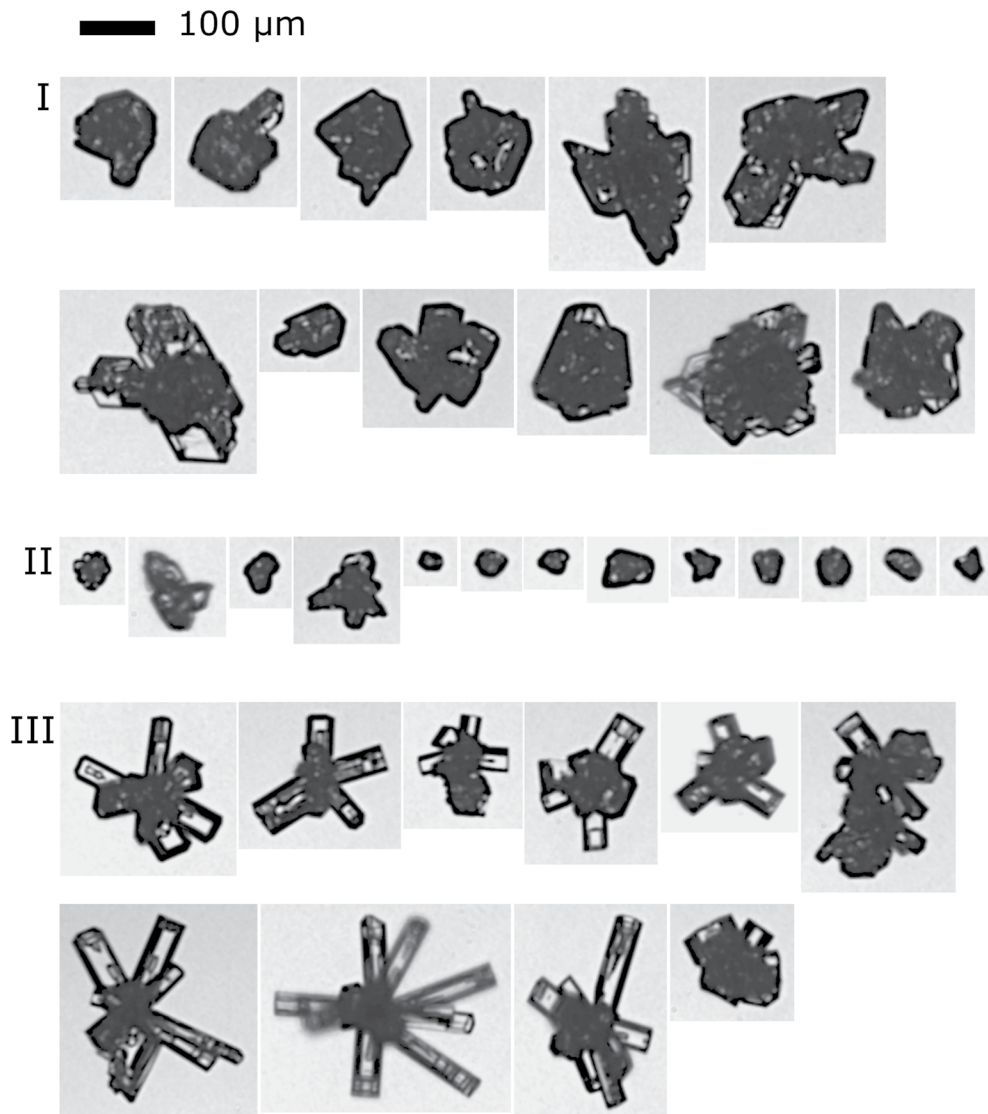

Figure 8. Example ice crystal images captured with the PHIPS probe from three periods shown in Figure 7.

The two highest sampling levels (around 11.3 km and −52°C) consisted of bullet rosettes with varying degree of complexity. Panel III in Figure 8 shows example crystals from a period between 11:41:30 and 11:41:54 UTC, when bullet rosettes with air inclusions and hollowness were observed. This period included 51 stereo-microscopic images, from which 78% were manually classified as bullet rosettes, 4% as irregular, 12% showed indication of shattering, one crystal was an individual bullet and the rest (4%) could not be classified. Later, around 11:43 UTC the bullet rosettes appeared increasing complex with side plane growth of varying degree.

The stereo-microscopic images indicated prevailing crystal complexities in the form of hollowness, surface roughness, air inclusions, and polycrystallinity. This is confirmed by the retrieved value of C_p, which was always above 0.4, also suggesting high accuracy of the retrieval of g. In addition, the particle size is generally above 50 μm, which corresponds to a size parameter around 295 at wavelength 532 nm. In accordance with Equation 32, the bias caused by geometric optics ray-tracing treatment is:

$$O\left(x^{-3/2}\right) = O\left(295^{-3/2}\right) = 10^{-4}, \tag{35}$$

which is small enough for accurate asymmetry parameter retrieval.

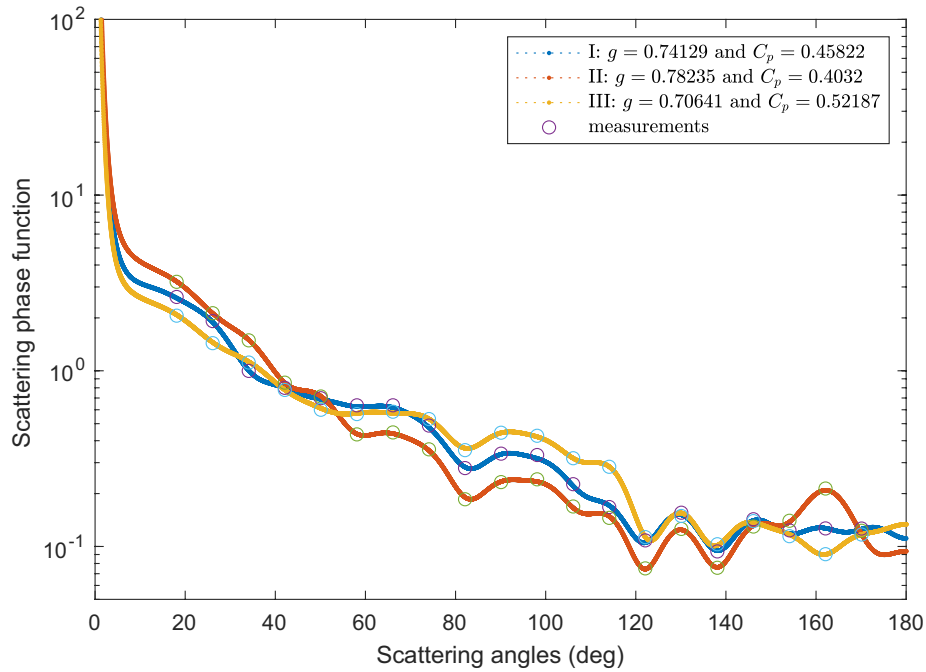

Figure 9. Three examples of extrapolated phase function and their asymmetry parameters and C_p values measured by PHIPS instrument, on June 29 2021. The measurements are indicated as open circles and are scaled to the phase function. The periods I, II, and III are highlighted in Figure 7 and example crystals corresponding to these periods are shown in Figure 8.

The algorithm described in Section 3 can be also used to recover the scattering phase function. Figure 9 displays the angular scattering function measurement and its extrapolation to whole angular range based on Equation 20 for the three periods shown in Figure 7. Note that the measurements are scaled such that its value at 42° matches the normalized phase function. Generally the peak of the normalized phase function will reach to the order of 10^5–10^6. The corresponding asymmetry parameter, g, and the value of C_p are displayed in the legends. It can be seen that lower retrieved g corresponds to a higher side- and backscattering intensity, as is expected. Because these phase functions are from direct in-situ measurement, they are potentially useful for radiative transfer simulations.

Figure 7d shows the retrieved values for g. Overall, the values for g vary between 0.67 and 0.78 with a median of 0.72 (Figure 10). No clear trend in g can be seen between the different altitudes or different crystal habits, which can be explained with the observed complexity of the ice crystals. Only during one period g values above 0.75 are observed. As discussed above, this period around 11:26 UTC showed small compact and quasi-spherical ice crystals occasionally in sub-saturated conditions. Therefore, the increase in g can be explained by decrease in the crystal complexity caused by sublimation of the crystals.

5.2. On the $g - C_p$ Relation

It has been well recognized that the asymmetry parameter and complexity of particle has some kinds of negative correlations. This relation is worthy of study in a more quantitative way because, among other factors (such as size), the complexity could play an important role in determining the asymmetry parameter of ice crystals. To our knowledge, such correlation has not been described in a uniform way. A major issue is that the definition of optical complexity of ice particle (model) is often dependent on specific models and methods, which makes the comparison between different optical models rather difficult, if not impossible. Since the asymmetry parameter is the first moment of scattering phase function, defining the "complexity" from the phase function moments seems to be reasonable and coherent.

The upper panel of Figure 10 displays the relations between the retrieved asymmetry parameter g and C_p. In total ~140 $g - C_p$ pairs are shown, indicating a clear negative correlation. In addition, we show the modeling curve

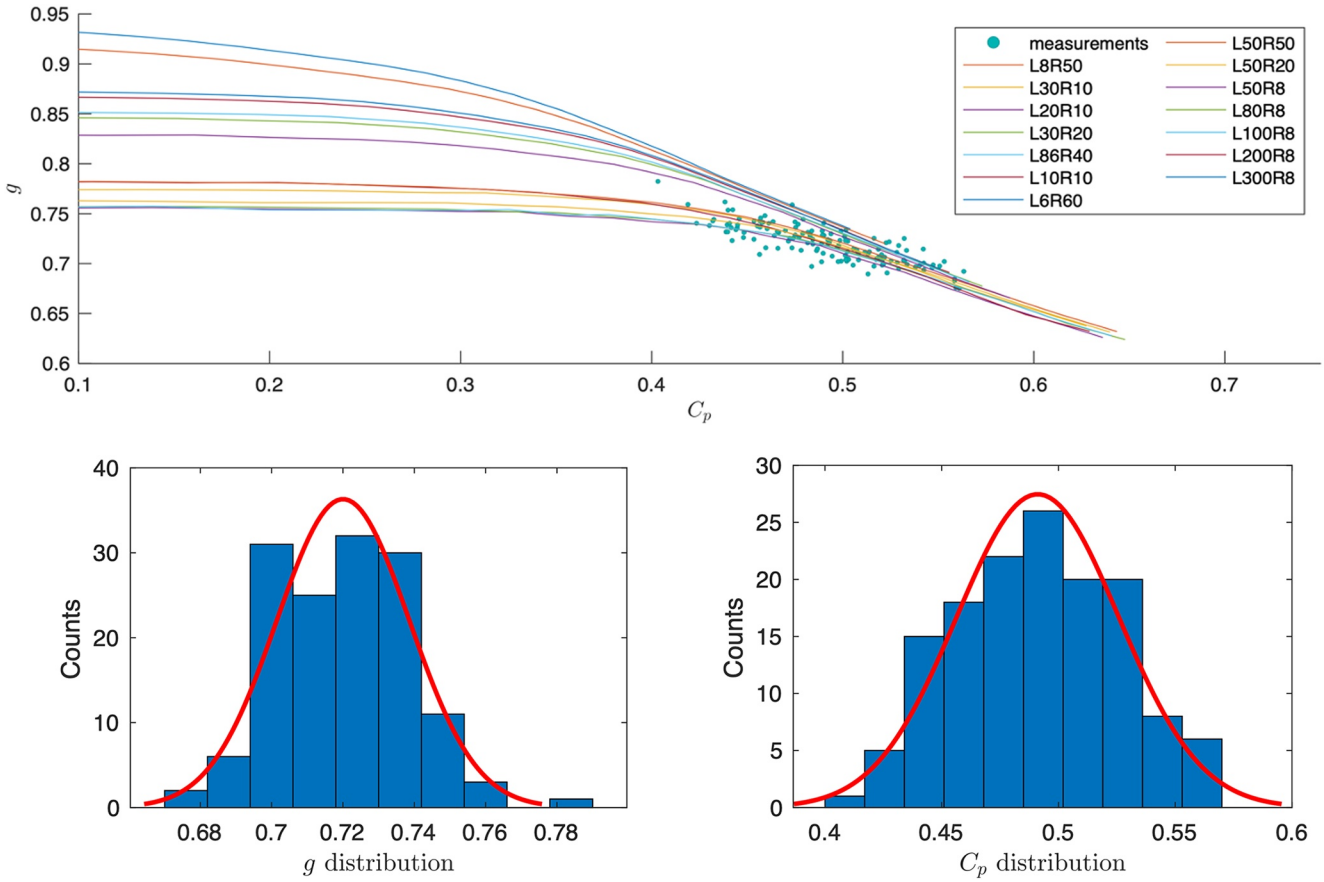

Figure 10. The relation between asymmetry parameter g and C_p in comparison with different scattering models. Based on data measured in CIRRUS-HL with PHIPS instrument, on June 29, 2021.

of hexagonal particle models with different aspect ratios. The high-aspect-ratio models (very flat plates or very long columns) correspond to those high-asymmetry-parameter curves in the low-C_p region. When the aspect ratio of the hexagonal model is close to unity, the asymmetry parameter seems to be insensitive to the increase of C_p. However, when the C_p becomes large enough, the asymmetry parameter of all particle models decreases in a similar rate. The retrieved data points of $g - C_p$ pairs are mostly concentrated in the high-C_p region (i.e., $C_p > 0.4$), suggesting high complexity of real ice crystals. It can be seen that the $g - C_p$ relation from the measurement matches well with the light scattering models.

The lower panels of Figure 10 show the histogram fitting of asymmetry parameter and the complexity parameter C_p, both displaying an approximate Gaussian profile. For asymmetry parameter, the mean value is $g = 0.720\ 0$, and the standard deviation is $\sigma = 0.018\ 6$, whereas the complexity parameter has a mean value of $C_p = 0.491\ 1$ and the standard deviation $\sigma = 0.034\ 8$. The distribution of C_p suggests that our result is within the region of high accuracy.

6. Conclusions

Accurately obtaining the asymmetry parameter of ice crystals is important for climate modeling, numerical scattering model development and atmospheric remote sensing. As a direct approach, in-situ measurements should be able to provide reliable ground truth. To improve the accuracy, we developed a novel and stable method for retrieving the asymmetry parameter from in-situ polar nephelometer measurements, that is, by fitting the measured angular scattering intensity with Legendre polynomials. Although we only conduct our measurement at single wavelength of 532 nm, accurate retrieval of the asymmetry parameter for a single wavelength in the visible band

is an important and necessary step toward accurately parameterizing the optical properties of ice crystals for climate modeling. The method is applicable to other visible wavelengths for other polar nephelometer instruments.

A key feature of the method is that it does not rely on any specific assumption about the truncated angular range in the near-forward scattering directions—an inherent problem of nephelometer measurements. In other words, it is a light scattering model-free approach and the asymmetry parameter is derived only based on measured data. This is achieved by exploiting the assumption that the forward *diffraction* and the *refraction* − *reflection* energies are asymptotically equal. By doing so, we manage to constrain the error of integration in accordance with the smoothness of the angular intensity distribution. The theoretical basis of this aproach links to the Gauss–Legendre quadrature, which is exact provided that the scattering phase function is smooth enough. As the scattering phase function becomes smooth, the nodes of Gauss–Legendre quadrature will be very well confined in the range of detection, and the assumption on the undetectable range become redundant. As a way of finding the best-fitting coefficients, the Gaussian integration method is both stable and accurate. For the geometric-optics treatment to be valid, however, it is only applicable to ice crystals with a characteristic length larger than 26 μm at a wavelength of 532 nm.

The parameter C_p has been introduced to characterize the smoothness of the phase function for the purpose of an error analysis. We also found a strong correlation between C_p and the distortion parameter used in the ray-tracing simulation. Therefore, C_p can also be used as an indicator of morphological complexity of ice crystals. It is found that as C_p reaches to 0.4, the retrieval becomes highly accurate. Although it is beyond the scope of this study, we note that experimental verification of the link between C_p and the complexity of ice crystals measured by some other instruments, such as the SID-3, is very much worthy of investigation in the future.

As an application, we analyzed a case study of Arctic cirrus from the recent airborne campaign CIRRUS-HL where polar nephelometer measurements were conducted using the PHIPS probe. The retrieved asymmetry parameter reveals clear negative correlation with C_p. The validity of our method is evident from the fact that the magnitude of C_p is generally above 0.4, which belongs to the region of high-accuracy. The median asymmetry parameter around 0.72 that was deduced from this Arctic cirrus case falls into the range between CIN measurements, Gerber et al. (2000); Garrett et al. (2001, 2003) and radiometric flux measurements Stephens et al. (1990) (see Table 1). The retrieved value of C_p (=0.49) suggests that real ice crystals could have much more complex morphology than the idealized models.

Data Availability Statement

Data used in the case study is from the CIRRUS-HL campaign. It can be accessed from https://halo-db.pa.op.dlr.de/. The retrieval algorithm for the asymmetry parameter is written in MATLAB. The code and part of the data is accessible at https://github.com/IMK-AAF-AG-Aircraft/Asymmetry-Parameter-Retrieval, under a MIT license.

Acknowledgments
We would like to thank the KIT group Airborne Cloud Observations and especially Shawn Wagner for preparing and operating the PHIPS probe during CIRRUS-HL. We also thank DLR for flight operations during CIRRUS-HL and Vladyslav Nenakhov and Christian Mallaun for preparing the BAHAMAS data used in Figure 7. This work was funded by the Helmholtz Association's Initiative and Networking Fund (grant agreement no. VH- NG-1531). Open access funding enabled and organized by Projekt DEAL.

References

Abdelmonem, A., Järvinen, E., Duft, D., Hirst, E., Vogt, S., Leisner, T., & Schnaiter, M. (2016). Phips–halo: The airborne particle habit imaging and polar scattering probe – Part 1: Design and operation. *Atmospheric Measurement Techniques*, *9*(7), 3131–3144. https://doi.org/10.5194/amt-9-3131-2016

Auriol, F., Gayet, J.-F., Febvre, G., Jourdan, O., Labonnote, L., & Brogniez, G. (2001). In situ observation of cirrus scattering phase functions with 22 and 46 halos: Cloud field study on 19 February 1998. *Journal of the Atmospheric Sciences*, *58*(22), 3376–3390. https://doi.org/10.1175/1520-0469(2001)058<3376:isoocs>2.0.co;2

Bacon, N. J., & Swanson, B. D. (2000). Laboratory measurements of light scattering by single levitated ice crystals. *Journal of the Atmospheric Sciences*, *57*(13), 2094–2104. https://doi.org/10.1175/1520-0469(2000)057<2094:lmolsb>2.0.co;2

Baumgardner, D., Abel, S., Axisa, D., Cotton, R., Crosier, J., & Field, P. (2017). Cloud ice properties: In situ measurement challenges. *Meteorological Monographs*, *58*, 9–1. https://doi.org/10.1175/amsmonographs-d-16-0011.1

Bi, L., & Yang, P. (2014). Accurate simulation of the optical properties of atmospheric ice crystals with the invariant imbedding t-matrix method. *Journal of Quantitative Spectroscopy and Radiative Transfer*, *138*, 17–35. https://doi.org/10.1016/j.jqsrt.2014.01.013

Bohren, C. F., & Huffman, D. R. (2008). *Absorption and scattering of light by small particles* (p. 110). John Wiley & Sons.

Diedenhoven, B. v., Cairns, B., Fridlind, A., Ackerman, A., & Garrett, T. (2013). Remote sensing of ice crystal asymmetry parameter using multi-directional polarization measurements–part 2: Application to the research scanning polarimeter. *Atmospheric Chemistry and Physics*, *13*(6), 3185–3203. https://doi.org/10.5194/acp-13-3185-2013

Diedenhoven, B. v., Cairns, B., Geogdzhayev, I., Fridlind, A., Ackerman, A., Yang, P., & Baum, B. (2012). Remote sensing of ice crystal asymmetry parameter using multi-directional polarization measurements–part 1: Methodology and evaluation with simulated measurements. *Atmospheric Measurement Techniques*, *5*(10), 2361–2374. https://doi.org/10.5194/amt-5-2361-2012

Fouquart, Y., Bonnel, B., & Ramaswamy, V. (1991). Intercomparing shortwave radiation codes for climate studies. *Journal of Geophysical Research: Atmospheres*, *96*(D5), 8955–8968. https://doi.org/10.1029/90jd00290

Fu, Q. (2007). A new parameterization of an asymmetry factor of cirrus clouds for climate models. *Journal of the Atmospheric Sciences*, *64*(11), 4140–4150. https://doi.org/10.1175/2007jas2289.1

Garrett, T. J., Gerber, H., Baumgardner, D. G., Twohy, C. H., & Weinstock, E. M. (2003). Small, highly reflective ice crystals in low-latitude cirrus. *Geophysical Research Letters*, *30*(21). https://doi.org/10.1029/2003gl018153

Garrett, T. J., Hobbs, P. V., & Gerber, H. (2001). Shortwave, single-scattering properties of arctic ice clouds. *Journal of Geophysical Research: Atmospheres*, *106*(D14), 15155–15172. https://doi.org/10.1029/2000jd900195

Gayet, J.-F., Auriol, F., Oshchepkov, S., Schröder, F., Duroure, C., Febvre, G., et al.(1998). In situ measurements of the scattering phase function of stratocumulus, contrails and cirrus. *Geophysical Research Letters*, *25*(7), 971–974. https://doi.org/10.1029/98GL00541

Gayet, J.-F., Ovarlez, J., Shcherbakov, V., Ström, J., Schumann, U., & Minikin, A. (2004). Cirrus cloud microphysical and optical properties at southern and northern midlatitudes during the inca experiment. *Journal of Geophysical Research: Atmospheres*, *109*(D20). https://doi.org/10.1029/2004jd004803

Gerber, H., Takano, Y., Garrett, T. J., & Hobbs, P. V. (2000). Nephelometer measurements of the asymmetry parameter, volume extinction coefficient, and backscatter ratio in arctic clouds. *Journal of the Atmospheric Sciences*, *57*(18), 3021–3034. https://doi.org/10.1175/1520-0469(2000)057<3021:nmotap>2.0.co;2

Hu, Y.-X., Wielicki, B., Lin, B., Gibson, G., Tsay, S.-C., Stamnes, K., & Wong, T. (2000). δ-Fit: A fast and accurate treatment of particle scattering phase functions with weighted singular-value decomposition least-squares fitting. *Journal of Quantitative Spectroscopy and Radiative Transfer*, *65*(4), 681–690. https://doi.org/10.1016/s0022-4073(99)00147-8

Iaquinta, J., Isaka, H., & Personne, P. (1995). Scattering phase function of bullet rosette ice crystals. *Journal of the Atmospheric Sciences*, *52*(9), 1401–1413. https://doi.org/10.1175/1520-0469(1995)052<1401:spfobr>2.0.co;2

Järvinen, E., Jourdan, O., Neubauer, D., Yao, B., Liu, C., & Andreae, M. O. (2018). Additional global climate cooling by clouds due to ice crystal complexity. *Atmospheric Chemistry and Physics*, *18*(21), 15767–15781. https://doi.org/10.5194/acp-18-15767-2018

Jourdan, O., Oshchepkov, S., Shcherbakov, V., Gayet, J.-F., & Isaka, H. (2003). Assessment of cloud optical parameters in the solar region: Retrievals from airborne measurements of scattering phase functions. *Journal of Geophysical Research: Atmospheres*, *108*(D18). https://doi.org/10.1029/2003jd003493

Kristjánsson, J., Edwards, J., & Mitchell, D. (2000). Impact of a new scheme for optical properties of ice crystals on climates of two GCMs. *Journal of Geophysical Research: Atmospheres*, *105*(D8), 10063–10079. https://doi.org/10.1029/2000jd900015

Labonnote, C.-L., Brogniez, G., Doutriaux-Boucher, M., Buriez, J.-C., Gayet, J.-F., & Chepfer, H. (2000). Modeling of light scattering in cirrus clouds with inhomogeneous hexagonal monocrystals. Comparison with in-situ and Adeos-polder measurements. *Geophysical Research Letters*, *27*(1), 113–116. https://doi.org/10.1029/1999gl010839

Liou, K.-N. (1986). Influence of cirrus clouds on weather and climate processes: A global perspective. *Monthly Weather Review*, *114*(6), 1167–1199. https://doi.org/10.1175/1520-0493(1986)114<1167:ioccow>2.0.co;2

Liou, K.-N. (1992). *Radiation and cloud processes in the atmosphere theory, observation, and modeling*.

Liou, K.-N. (2002). *An introduction to atmospheric radiation*. Elsevier.

Liou, K.-N., & Yang, P. (2016). *Light scattering by ice crystals: Fundamentals and applications*. Cambridge University Press.

Liu, C., Yang, P., Minnis, P., Loeb, N., Kato, S., Heymsfield, A., & Schmitt, C. (2014). A two-habit model for the microphysical and optical properties of ice clouds. *Atmospheric Chemistry and Physics*, *14*(24), 13719–13737. https://doi.org/10.5194/acp-14-13719-2014

Mace, G. G., Zhang, Q., Vaughan, M., Marchand, R., Stephens, G., Trepte, C., & Winker, D. (2009). A description of hydrometeor layer occurrence statistics derived from the first year of merged Cloudsat and Calipso data. *Journal of Geophysical Research: Atmospheres*, *114*(D8). https://doi.org/10.1029/2007jd009755

Macke, A., Francis, P. N., McFarquhar, G. M., & Kinne, S. (1998). The role of ice particle shapes and size distributions in the single scattering properties of cirrus clouds. *Journal of the Atmospheric Sciences*, *55*(17), 2874–2883. https://doi.org/10.1175/1520-0469(1998)055<2874:troips>2.0.co;2

Macke, A., Mueller, J., & Raschke, E. (1996). Single scattering properties of atmospheric ice crystals. *Journal of the Atmospheric Sciences*, *53*(19), 2813–2825. https://doi.org/10.1175/1520-0469(1996)053<2813:sspoai>2.0.co;2

Matus, A. V., & L'Ecuyer, T. S. (2017). The role of cloud phase in earth's radiation budget. *Journal of Geophysical Research: Atmospheres*, *122*(5), 2559–2578. https://doi.org/10.1002/2016jd025951

Meador, W., & Weaver, W. (1980). Two-stream approximations to radiative transfer in planetary atmospheres: A unified description of existing methods and a new improvement. *Journal of the Atmospheric Sciences*, *37*(3), 630–643. https://doi.org/10.1175/1520-0469(1980)037<0630:tsatrt>2.0.co;2

Mioche, G., Josset, D., Gayet, J.-F., Pelon, J., Garnier, A., Minikin, A., & Schwarzenboeck, A. (2010). Validation of the CALIPSO-caliop extinction coefficients from in situ observations in midlatitude cirrus clouds during the circle-2 experiment. *Journal of Geophysical Research: Atmospheres*, *115*(D4). https://doi.org/10.1029/2009jd012376

Mishchenko, M. I., Travis, L. D., & Lacis, A. A. (2002). *Scattering, absorption, and emission of light by small particles*. Cambridge University Press.

Mishchenko, M. I., Travis, L. D., & Mackowski, D. W. (1996). T-Matrix computations of light scattering by nonspherical particles: A review. *Journal of Quantitative Spectroscopy and Radiative Transfer*, *55*(5), 535–575. https://doi.org/10.1016/0022-4073(96)00002-7

Muinonen, K., Nousiainen, T., Fast, P., Lumme, K., & Peltoniemi, J. (1996). Light scattering by Gaussian random particles: Ray optics approximation. *Journal of Quantitative Spectroscopy and Radiative Transfer*, *55*(5), 577–601. https://doi.org/10.1016/0022-4073(96)00003-9

Randles, C. A., Kinne, S., Myhre, G., Schulz, M., Stier, P., & Fischer, J. (2013). Intercomparison of shortwave radiative transfer schemes in global aerosol modeling: Results from the aerocom radiative transfer experiment. *Atmospheric Chemistry and Physics*, *13*(5), 2347–2379. https://doi.org/10.5194/acp-13-2347-2013

Sassen, K., Wang, Z., & Liu, D. (2008). Global distribution of cirrus clouds from Cloudsat/cloud-aerosol Lidar and infrared pathfinder satellite observations (calipso) measurements. *Journal of Geophysical Research: Atmospheres*, *113*(D8). https://doi.org/10.1029/2008jd009972

Schnaiter, M., Järvinen, E., Abdelmonem, A., & Leisner, T. (2018). Phips-halo: The airborne particle habit imaging and polar scattering probe – Part 2: Characterization and first results. *Atmospheric Measurement Techniques*, *11*(1), 341–357. https://doi.org/10.5194/amt-11-341-2018

Shcherbakov, V., Gayet, J.-F., Jourdan, O., Minikin, A., Ström, J., & Petzold, A. (2005). Assessment of cirrus cloud optical and microphysical data reliability by applying statistical procedures. *Journal of Atmospheric and Oceanic Technology*, *22*(4), 409–420. https://doi.org/10.1175/jtech1710.1

Shiobara, M., & Asano, S. (1994). Estimation of cirrus optical thickness from sun photometer measurements. *Journal of Applied Meteorology and Climatology*, *33*(6), 672–681. https://doi.org/10.1175/1520-0450(1994)033<0672:eocotf>2.0.co;2

Stackhouse, P. W., Jr, & Stephens, G. L. (1991). A theoretical and observational study of the radiative properties of cirrus: Results from fire 1986. *Journal of the Atmospheric Sciences*, *48*(18), 2044–2059. https://doi.org/10.1175/1520-0469(1991)048<2044:ataoso>2.0.co;2

Stephens, G. L., Tsay, S.-C., Stackhouse, P. W., Jr, & Flatau, P. J. (1990). The relevance of the microphysical and radiative properties of cirrus clouds to climate and climatic feedback. *Journal of the Atmospheric Sciences*, *47*(14), 1742–1754. https://doi.org/10.1175/1520-0469(1990)047<1742:trotma>2.0.co;2

Taflove, A., & Umashankar, K. R. (1990). The finite-difference time-domain method for numerical modeling of electromagnetic wave interactions. *Electromagnetics*, *10*(1–2), 105–126. https://doi.org/10.1080/02726349008908231

van de Hulst, H. C. (1980). *Multiple light scattering*. Elsevier.

van Diedenhoven, B., Ackerman, A. S., Cairns, B., & Fridlind, A. M. (2014). A flexible parameterization for shortwave optical properties of ice crystals. *Journal of the Atmospheric Sciences*, *71*(5), 1763–1782. https://doi.org/10.1175/jas-d-13-0205.1

Wielicki, B. A., Suttles, J. T., Heymsfield, A. J., Welch, R. M., Spinhirne, J. D., & Wu, M.-L. C. (1990). The 27–28 October 1986 FIRF IFO cirrus case study: Comparison of radiative transfer theory with observations by satellite and aircraft. *Monthly Weather Review*, *118*(11), 2356–2376. https://doi.org/10.1175/1520-0493(1990)118<2356:toficc>2.0.co;2

Wiscombe, W. (1977). The delta–m method: Rapid yet accurate radiative flux calculations for strongly asymmetric phase functions. *Journal of the Atmospheric Sciences*, *34*(9), 1408–1422. https://doi.org/10.1175/1520-0469(1977)034<1408:tdmrya>2.0.co;2

Yang, P., Bi, L., Baum, B. A., Liou, K.-N., Kattawar, G. W., Mishchenko, M. I., & Cole, B. (2013). Spectrally consistent scattering, absorption, and polarization properties of atmospheric ice crystals at wavelengths from 0.2 to 100 μ m. *Journal of the Atmospheric Sciences*, *70*(1), 330–347. https://doi.org/10.1175/jas-d-12-039.1

Yang, P., Hioki, S., Saito, M., Kuo, C.-P., Baum, B., & Liou, K.-N. (2018). A review of ice cloud optical property models for passive satellite remote sensing. *Atmosphere*, *9*(12), 499. https://doi.org/10.3390/atmos9120499

Yang, P., Kattawar, G. W., Hong, G., Minnis, P., & Hu, Y. (2008). Uncertainties associated with the surface texture of ice particles in satellite-based retrieval of cirrus clouds—Part i: Single-scattering properties of ice crystals with surface roughness. *IEEE Transactions on Geoscience and Remote Sensing*, *46*(7), 1940–1947. https://doi.org/10.1109/tgrs.2008.916471

Yang, P., & Liou, K. (1996a). Finite-difference time domain method for light scattering by small ice crystals in three-dimensional space. *JOSA A*, *13*(10), 2072–2085. https://doi.org/10.1364/josaa.13.002072

Yang, P., & Liou, K. (1996b). Geometric-optics–integral-equation method for light scattering by nonspherical ice crystals. *Applied Optics*, *35*(33), 6568–6584. https://doi.org/10.1364/ao.35.006568

Yurkin, M. A., Hoekstra, A. G., Brock, R. S., & Lu, J. Q. (2007). Systematic comparison of the discrete dipole approximation and the finite difference time domain method for large dielectric scatterers. *Optics Express*, *15*(26), 17902–17911. https://doi.org/10.1364/oe.15.017902